



## A warm layer in the nightside mesosphere of Mars

Hiromu Nakagawa, Sonal K. Jain, Nicholas M. Schneider, Franck Montmessin, Roger V. Yelle, F. Jiang, Loïc Verdier, Takeshi Kuroda, Nao Yoshida, Hitoshi Fujiwara, et al.

### ► To cite this version:

Hiromu Nakagawa, Sonal K. Jain, Nicholas M. Schneider, Franck Montmessin, Roger V. Yelle, et al.. A warm layer in the nightside mesosphere of Mars. *Geophysical Research Letters*, 2020, 47 (4), pp.e2019GL085646. 10.1029/2019GL085646 . insu-02476853

HAL Id: insu-02476853

<https://insu.hal.science/insu-02476853>

Submitted on 29 Mar 2021

**HAL** is a multi-disciplinary open access archive for the deposit and dissemination of scientific research documents, whether they are published or not. The documents may come from teaching and research institutions in France or abroad, or from public or private research centers.

L'archive ouverte pluridisciplinaire **HAL**, est destinée au dépôt et à la diffusion de documents scientifiques de niveau recherche, publiés ou non, émanant des établissements d'enseignement et de recherche français ou étrangers, des laboratoires publics ou privés.

# Geophysical Research Letters

## RESEARCH LETTER

10.1029/2019GL085646

### Key Points:

- MAVEN/IUVS revealed a warm layer between 70 and 90 km altitude in the nightside on Mars during  $L_s = 0\text{--}180^\circ$  in Martian Year 33–34
- The observed peak temperature amplitudes of nightside profiles are higher than those predicted by the model by up to 90 K
- Longitudinal wavenumber-3 structures are seen in the warm layer, two times larger amplitudes than predicted

### Correspondence to:

H. Nakagawa,  
hnakagawa@tohoku.ac.jp

### Citation:

Nakagawa, H., Jain, S. K., Schneider, N. M., Montmessin, F., Yelle, R. V., Jiang, F., et al. (2020). A warm layer in the nightside mesosphere of Mars. *Geophysical Research Letters*, 47, e2019GL085646. <https://doi.org/10.1029/2019GL085646>

Received 2 OCT 2019

Accepted 11 FEB 2020

Accepted article online 12 FEB 2020

## A Warm Layer in the Nightside Mesosphere of Mars

Hiromu Nakagawa<sup>1</sup> , Sonal K. Jain<sup>2</sup> , Nicholas M. Schneider<sup>2</sup> , Franck Montmessin<sup>3</sup> , Roger V. Yelle<sup>4</sup> , Fanyu Jiang<sup>4</sup>, Loic Verdier<sup>3</sup>, Takeshi Kuroda<sup>1</sup> , Nao Yoshida<sup>1</sup> , Hitoshi Fujiwara<sup>5</sup>, Takeshi Imamura<sup>6</sup> , Naoki Terada<sup>1</sup> , Kaori Terada<sup>1</sup> , Kanako Seki<sup>7</sup> , Hannes Gröller<sup>4</sup> , and Justin I. Deighan<sup>2</sup> 

<sup>1</sup>Graduate School of Science, Tohoku University, Sendai, Japan, <sup>2</sup>Laboratory for Atmospheric and Space Physics, University of Colorado, Boulder, CO, USA, <sup>3</sup>Laboratoire Atmosphères, Milieux, Observations Spatiales (LATMOS), UVSQ Université Paris-Saclay, Sorbonne Université, CNES, Paris, France, <sup>4</sup>Lunar and Planetary Laboratory, University of Arizona, Tucson, AZ, USA, <sup>5</sup>Faculty of Science and Technology, Seikei University, Tokyo, Japan, <sup>6</sup>Graduate School of Frontier Sciences, The University of Tokyo, Tokyo, Japan, <sup>7</sup>Graduate School of Science, The University of Tokyo, Tokyo, Japan

**Abstract** We report a new set of stellar occultation measurements for nightside temperature profiles made by the Mars Atmosphere and Volatile EvolutioN/Imaging Ultraviolet Spectrograph that provide evidence for a recurring layer of warm air between 70 and 90 km altitudes in the nightside mesosphere of Mars during  $L_s = 0\text{--}180^\circ$  in Martian Year 33–34. The nightside profiles reveal a recurring peak of atmospheric temperature around 80 km over the equator to the middle latitudes in the northern hemisphere. The predictions of the Mars Climate Database have a warm layer with much smaller amplitudes. The observed peak amplitudes are larger than those predicted by the model by up to 90 K. Wavenumber-3 structures are seen in the warm layer that are potentially signatures of thermal tides or stationary planetary waves, with amplitudes two times larger than predicted.

**Plain Language Summary** The Mars middle atmosphere is an intermediate region with rich and complex dynamics influenced by the underlying lower atmosphere and the overlying upper atmosphere. We report a new set of stellar occultation measurements made by the MAVEN/IUVS that provide evidence for a warm layer between 70 and 90 km altitude in the nightside mesosphere of Mars during  $L_s = 0\text{--}180^\circ$  in Martian Year 33–34.

## 1. Introduction

The Mars middle atmosphere is well-known as an intermediate atmospheric region strongly influenced by coupling with the underlying lower atmosphere (via gravity waves, planetary waves and tides, and dust storms) and coupling with the overlying upper atmosphere and ultimately the Sun (via solar extreme ultraviolet radiation and solar wind particles) (e.g., Bouger et al., 2002, 2008, 2014, 2015; Gonzalez-Galindo et al., 2015, 2018). On the other hand, the Martian middle atmosphere remains the least explored region with a highly variable nature that deserves extensive measurements.

The density and thermal structures of the Martian lower atmosphere, up to 50 km, have been investigated by the thermal infrared spectrometers and the radio science experiments onboard Mars Global Surveyor (Hinson et al., 2004; Smith, 2004; Smith et al., 2001) and Mars Express (Grassi et al., 2005; Pätzold et al., 2016). Mars Climate Sounder onboard Mars Reconnaissance Orbiter (McCleese et al., 2007) extended the observed range up to 80 km. Above this level, a few in situ measurements are available, including the density profiles from the Viking, Pathfinder, and Mars Exploration Rovers (Magalhães et al., 1999; Seiff & Kirk, 1977; Withers & Smith, 2006) and the density measurements obtained during the aerobraking phases of the Mars Global Surveyor, Mars Odyssey, and Mars Reconnaissance Orbiter missions (Keating et al., 1998, 2003, 2007). These observations have revealed rich and complex dynamics combining various kinds of waves probably interacting with the mean circulation (Forbes et al., 2002; Magalhães et al., 1999).

The solar and stellar occultation technique applied to the Martian atmosphere with the Mars Express spectrometer Spectroscopy for Investigation of Characteristics of the Atmosphere of Mars (SPICAM) measures the atmospheric transmission from which information about the vertical structure and composition in the 60–130 km region can be derived (Bertaux et al., 2006; Forget et al., 1999; Montmessin et al., 2006;

Quémérais et al., 2006). SPICAM provided information about aerosols and clouds (Montmessin et al., 2006; Määttänen et al., 2013), ozone (Lebonnois et al., 2006; Määttänen et al., 2019; Modak et al., 2019), density and temperature (Forget et al., 1999, 2009), tides (Withers et al., 2011), and eventually O<sub>2</sub> (Sandel et al., 2015). Forget et al. (2009) and Gonzalez-Galindo et al. (2018) investigated latitudinal and seasonal variations of observed density and temperature in the middle atmosphere. Montmessin et al. (2017) give an overview of results from SPICAM observations.

SPICAM occultation has recently revealed an unexpected high abundance of water vapor in the middle atmosphere that supposedly drives the enhancement of the atomic hydrogen escape (Chaffin et al., 2017; Fedorova et al., 2018; Heavens et al., 2018; Maltagliati et al., 2011, 2013). However, it is unclear how to extract water vapor from the lower atmosphere and place it in the middle atmosphere since water vapor is limited in its vertical propagation by the cold trap of its condensation level; the cold trap leads to water freezing out, confining water in the lower atmosphere. It has been proposed that an inflation of the lower atmosphere due to the sunlight absorbed by the upsurge of dust associated with intensified meridional circulation can transport water vapor effectively into the middle atmosphere (Fedorova et al., 2018). Recent observations of dust, water, and semiheavy water (HDO) by the NOMAD and ACS onboard the ExoMars Trace Gas Orbiter also propose that the increase of water abundances may be the result of warmer temperatures during the dust storm causing stronger atmospheric circulation and preventing ice cloud formation (Vandaele et al., 2019). The background temperature profiles are the key to understand how to preserve the detached layer of the water vapor in the middle atmosphere. However, a comprehensive picture of the thermal structure and dynamics in the middle atmosphere is yet to be established.

Here, we report new stellar occultation observations by the Imaging Ultraviolet Spectrograph (IUVS) onboard the Mars Atmosphere and Volatile EvolutioN (MAVEN) mission, which allows us to study the vertical structure of the atmospheric temperature in the 20–140 km altitude region (Gröller et al., 2015, 2018) in a way similar to SPICAM but with a more complete coverage in latitude, longitude, and season on the nightside.

## 2. Observations

The IUVS instrument and its various modes of operation were described by McClintock et al. (2014), while the technique of stellar occultation and the processing of the IUVS observations are described by Gröller et al. (2015, 2018). During an occultation, IUVS continuously observes a selected star, while the spacecraft moves around the planet so that the star setting or rising through the atmosphere is observed. When the star is seen through the atmosphere, the spectrum is modified by the absorption of all atmospheric constituents integrated along the line of sight from the star to the instrument. Occultations are performed during campaigns lasting 1 to 2 days. Repeated measurements of a particular star provide measurements at essentially constant latitudes and local times (LTs) at different longitudes. A campaign of observations during consecutive orbits roughly samples all longitudes. The targeted UV-bright stars were selected for providing a certain latitude and LT coverage at a certain season over 3 years. A well-controlled Articulated Payload Platform on the MAVEN enables the specific pointing of the instrument to any star, thus enabling IUVS with good spatial coverage. We restrict our analysis to 19 stellar occultation campaigns separated by 2–3 months. IUVS measures the 110–340 nm wavelength region in two channels: the FUV at 110–190 nm and the MUV at 180–340 nm. The use of two channels provides high sensitivity and spectral resolution, ensuring detection of CO<sub>2</sub>, O<sub>2</sub>, and O<sub>3</sub> densities, aerosol opacity, and subsequently, (from the CO<sub>2</sub> density profile) the thermal structure in 20–140 km altitude range. Temperature profiles have been derived from the density profiles assuming that the atmosphere is in hydrostatic equilibrium. Our inferred temperature profiles have a typical vertical resolution of 2 to 10 km, which is smaller than or equal to the average atmospheric scale height (6–12 km, depending on altitude). We consider only nightside occultation (LT = 0–6 hr, 18–24 hr) where sunlight scattered by aerosols and reflected by the surface do not affect the measurements. The list of the stellar occultation campaigns presented in this study is summarized in Table 1. We confine our analysis to 188 nightside temperature profiles that have altitude coverage probing below 60 km and whose uncertainty is less than 20 % of the background during the period from 24 March 2015 to 12 April 2018 (98 profiles in L<sub>s</sub> = 0–90°, and 90 profiles in L<sub>s</sub> = 90–180°). All density and temperature profiles used in this study correspond to level 2, version 13, revision 1 data provided by the Planetary Data System (PDS). The filename in the PDS contains

**Table 1***List of the Stellar Occultation Campaigns Applied for this Study*

Campaign	Date	MY (Sols)	Orbit	$L_s$	Used (total)
#3	1–2 August 2015	33 (43)	01635-01640	22	11 (37)
#5	3–4 November 2015	33 (134)	02132-02137	64	15 (29)
#7	17–18 March 2016	33 (265)	02848-02853	124	25 (39)
#8	26–27 May 2016	33 (334)	03223-03228	159	3 (38)
#14	14–15 June 2017	34 (39)	05246-05254	19	17 (27)
#15	5–7 July 2017	34 (59)	05357-05366	29	28 (36)
#16	8–9 October 2017	34 (152)	05866-05875	71	27 (27)
#17	6–8 December 2017	34 (209)	06193-06202	97	25 (53)
#18	7–9 February 2018	34 (270)	06532-06541	126	12 (55)
#19	11–12 April 2018	34 (332)	06866-06875	157	25 (57)
Total number of profiles					188 (398)

the keywords, occultation, level 2, version 13, which enables to identify the data set. In this study, IUVS observations are compared with simulations by Mars Climate Database (MCD) version 5.3. (Millour et al., 2012).

### 3. Results

Analysis of the 188 nightside profiles has identified a pattern of recurring high-altitude warm layers under various season and latitudinal conditions. Figure 1 shows a selection of profiles representing a warm layer in the middle atmosphere during the period from  $L_s = 0$ –180°. The geographic distribution of tangential footprints of the IUVS stellar occultations, season, and targeted stars is given in each panel. The geometric tangential footprint refers the near point for each occultation. These profiles exhibit a recurring layer of warm air at a similar pressure level, approximately at altitudes 70–90 km. Such warm air in this altitude range is the most surprising result of this work, not expected by classical theory.

In Figure 1, the IUVS profiles were compared with the MCD (as the broken lines) using an average condition of solar extreme ultraviolet. The predicted temperature profiles by the MCD gradually decreases from ~150 K around 40 km to ~100 K above 100 km. The comparison reveals a relatively good match between the IUVS and the MCD, except for the distinct feature of warm layer in the 70–90 km range. The temperature around 80 km predicted by the MCD underestimates the observed temperature by up to 90 K. It is noteworthy that the MCD predictions also indicate small bumps at altitude ranges shown in Figure 1 with low peak values up to 160 K. These bumps could be associated with the upward propagating thermal tides. The predicted profiles by MCD, however, do not show a significant increase of the amplitudes around 80–100 km altitude. The contrast of warm layer amplitudes between the IUVS and the MCD is striking.

The geographic distribution of nightside occultations applied in this study is represented in Figures 2a–2c. The geometrical parameters of tangential footprints of the occultation evolved throughout the mission. Thus, the results shown here represent a combination of these geometrical variations with actual atmospheric variations. The sufficient coverage in longitude and latitude is visible, except for the northern high-latitude region. The red dots correspond to profiles representing the warm layers in the middle atmosphere; meanwhile, the blues correspond to featureless profiles. Here, the criteria for the detection of the warm layer are (i) temperature maximum in 60–100 km larger than 170 K and (ii) warmer values than the background profile led by the second-order polynomial fit to the profile of more than 15 K. Detection by these criteria coincides with that by visual judgment. In Figures 2a–2c, the recurring detections of the warm layer over the equator to the middle latitudes in the northern hemisphere are obvious, in addition to the southern high latitudes. On the other hand, a lack of detections of warm layers in the southern middle latitudes is apparent.

By collecting the nightside profiles from  $L_s = 0$ –180°, a latitude-altitude cross section of the zonally averaged atmospheric temperature is obtained as shown in Figure 2d. The number of profiles per bin ranges from 4 to 23. The total number of profiles is 188 for the map. The standard deviation computed for each bin is 16.7 K in average, which is smaller than the amplitude of the observed feature. An enhancement of temperature in the

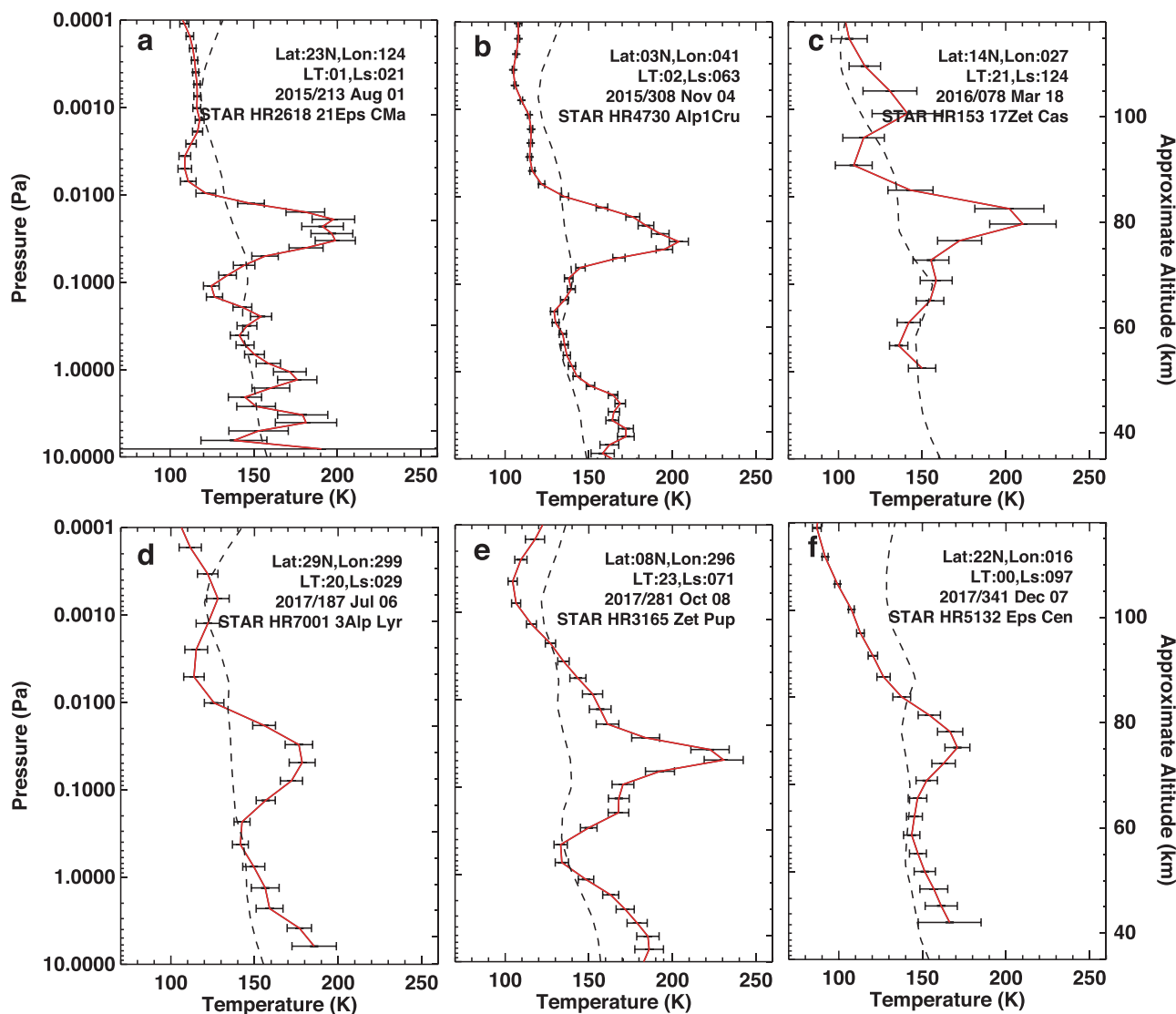


**Figure 1.** Examples of profiles representing the warm layers in the middle atmosphere. The geometric locations of tangential footprints of the Imaging Ultraviolet Spectrograph stellar occultation measurements, seasons, and targeted stars are shown in each panel. The geometric tangential footprint refers the near point for each occultation. The predicted temperature profiles were shown as dashed lines in panels from the Mars Climate Database v5.3 using an average condition of solar extreme ultraviolet and a typical dust climatology for corresponding geometries of Imaging Ultraviolet Spectrograph.

middle atmosphere above the southern winter pole is nonetheless obvious, labeled region A in Figure 2d, but is apparently caused by the polar warming found in the winter hemisphere (McCauley et al., 2008). However, there is no explanation for the strong warm layer observed by IUVS in the northern summer mesosphere, labeled region B in Figure 2d. Our results suggest the presence of a recurring peak of temperature at 80 km at the equator to the middle latitudes in the northern hemisphere, whereas this peak is not observed in the middle latitudes of the southern hemisphere. Statistical study during  $L_s = 0-180^\circ$  proves that the warm layer is not an observational artifact.

Longitudinal cross sections of temperature averaged over  $L_s = 0-180^\circ$  in the northern hemisphere ( $0^\circ$  to  $50^\circ\text{N}$ ) and the southern hemisphere ( $50^\circ\text{S}$  to  $0^\circ$ ) are presented on the nightside in Figure 3. We find concentrations of warm maxima roughly around the longitudes  $20^\circ$ ,  $140^\circ$ , and  $300^\circ$ , which exceed 200 K, in Figure 3a. This has a similar characteristic to the wavenumber-3 structure found in the mesosphere-thermosphere by previous studies (e.g., England et al., 2016, 2019; Gröller et al., 2018; Stiepen et al., 2017). The temperature at altitudes 75–85 km are extracted to show longitudinal variations in Figure 4 with the wavenumber-0 to -3 least squares fit to those data, as was similarly done in the previous studies (e.g., England et al., 2016, 2019; Gröller et al., 2018).

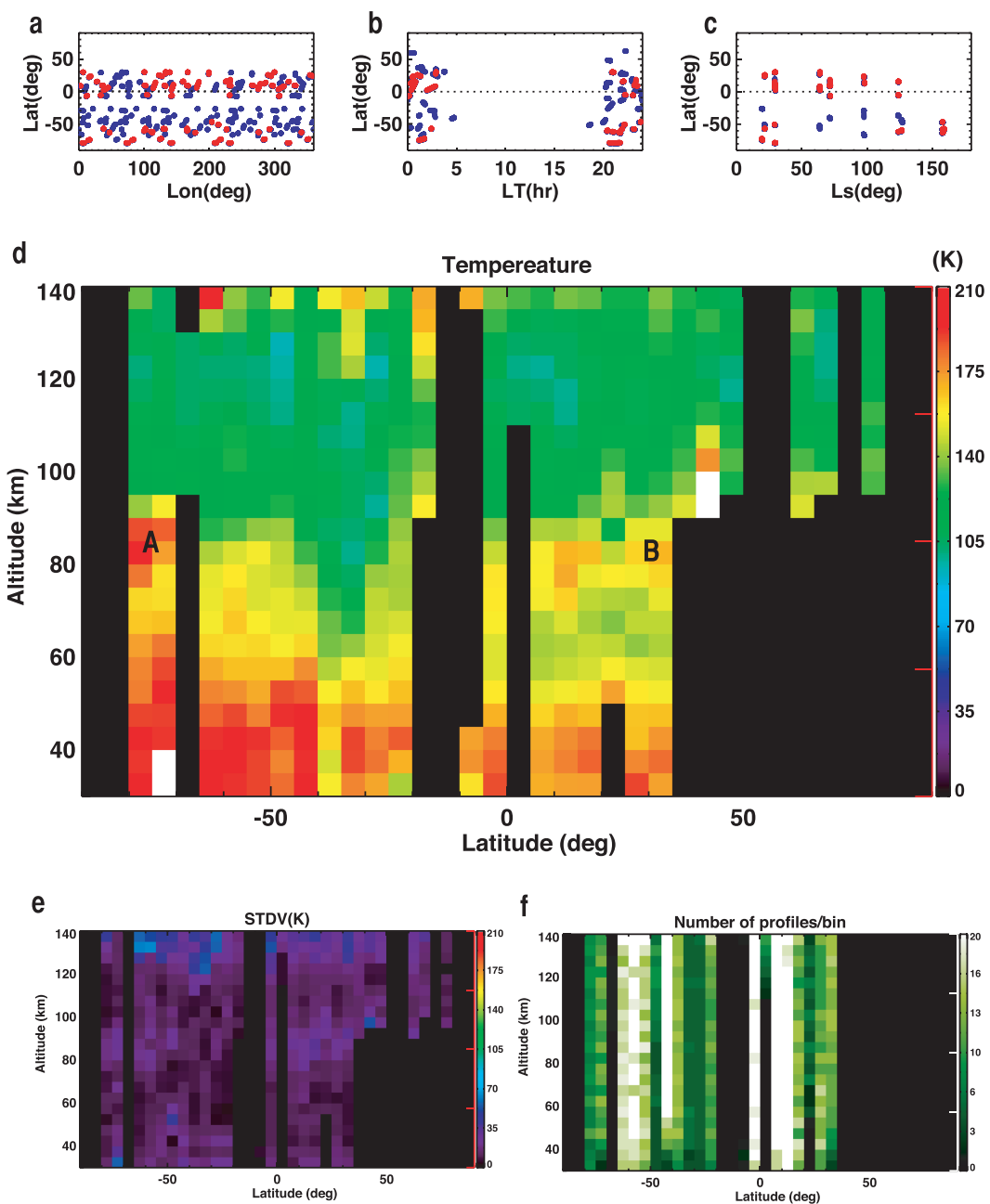


**Figure 2.** The geometric locations in latitude versus (a) longitude, (b) local time, and (c) season of tangential footprints of the Imaging Ultraviolet Spectrograph stellar occultation measurements applied in the study from  $L_s = 0-180^\circ$  are shown. The red corresponds to profiles representing the warm layers in the middle atmosphere. The blue corresponds to featureless profiles. The criteria are described in the text. Latitude-altitude cross section of zonally averaged atmospheric temperature over  $L_s = 0-180^\circ$  is shown in panel (d). The temperatures were averaged over the altitude bins of 5 km and latitude bins of  $5^\circ$ . Regions A and B highlight the mesospheric warming described in the text. The standard deviations of averaged temperature for each bin are shown in the panel (e). The number of profiles for each bin are shown in the panel (f). The number of profiles is 188 in total for the map.

The relative amplitudes of the wavenumber-1 to -3 components are 2.1, 2.4, and 10.5 K, respectively, in IUVS data. The standard deviation from the fit is (a) 28.7 K, (b) 22.2 K, (c) 10.3 K, and (d) 10.6 K, respectively. The amplitudes revealed a wavenumber-3 structure that is dominant with significant amplitudes. This is comparable to wavenumber-3 signatures found by previous observations in the middle atmosphere that have been interpreted as signatures of diurnal and semidiurnal tides or stationary planetary waves (Stiepen et al., 2017; England et al., 2016, 2019). This suggests that the possible atmospheric waves force

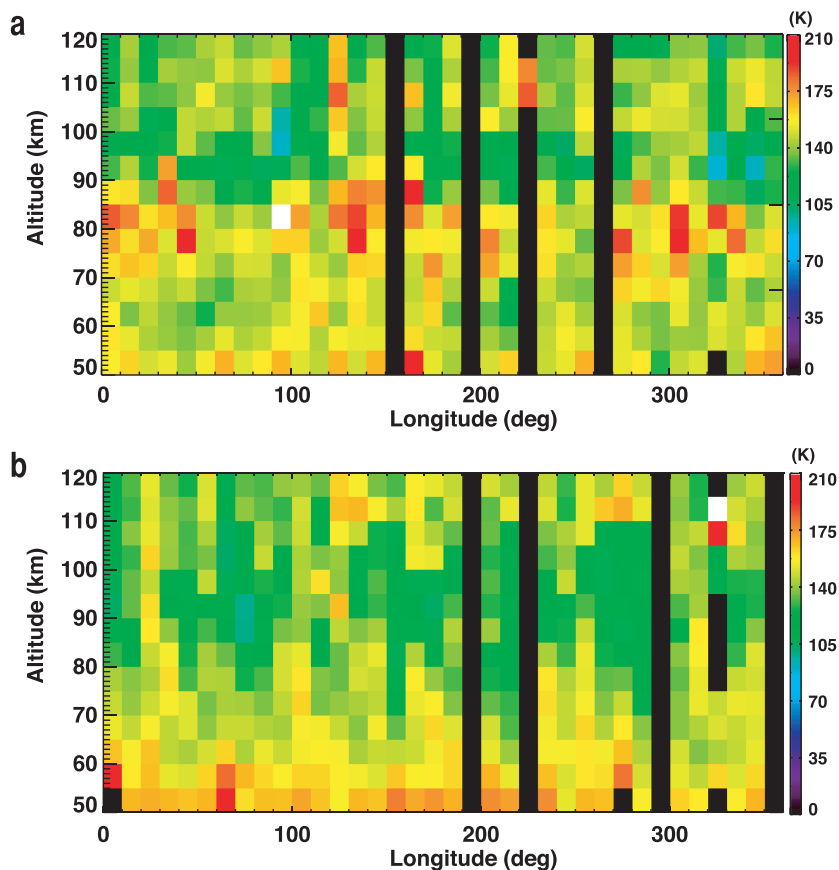


**Figure 3.** Longitude-altitude cross section of averaged atmospheric temperature over  $L_s = 0\text{--}180^\circ$  (a) from  $0^\circ$  to  $50^\circ\text{N}$  latitude and from (b)  $50^\circ\text{S}$  to  $0^\circ$  latitude. The temperatures were averaged over altitude bins of 5 km and longitude bins of  $5^\circ$ . The total number of profiles in the map is 57 from  $0^\circ$  to  $50^\circ\text{N}$  latitude and 68 from  $50^\circ\text{S}$  to  $0^\circ$  latitude.

longitudinal variability of thermal structure in the middle atmosphere. Longitudinal variations of nitric oxide (NO) nightglow reported by Stiepen et al. (2017) show a comparable signature, which seems to be in phase with those found in this study. These waves apparently have an impact on the amplitude of the warm layer. Longitudinal variation in the model prediction also indicates the wave-3 structure but with much smaller amplitudes. It is noteworthy that the model prediction coincides with observation in phase quite well. In contrast, the southern hemisphere is featureless in both IUVS and MCD. Although IUVS shows more highly variable nature in this altitude range, the MCD reasonably matches with the IUVS in general. The approximate ratios between the observed variation and the modeled were estimated to be 1.14 with a standard deviation of 0.17 in the northern hemisphere and 0.96 with a standard deviation of 0.18 in the southern hemisphere.

#### 4. Discussion

Our results reveal the presence of a strong temperature inversion layer in the mesosphere at northern summer low latitudes. It is also indicated in Heavens et al. (2010), possibly due to the upward-propagating atmospheric waves from below, such as small-scale gravity waves (Fritts & Alexander, 2003). They potentially break in the mesosphere, then deposit their horizontal momentum into the background mean winds and change the mean wind velocity. If there are the convective instabilities related to the temperature inversion, they could also create a turbulence layer. The vertical mixing induced by the turbulence layer might also influence the homopause and thereby thermospheric composition.

The discovery of an unexpected temperature gradient in the nightside mesosphere, with a distinct layer of warm air which has never been explained, would affect our current understanding of the Martian

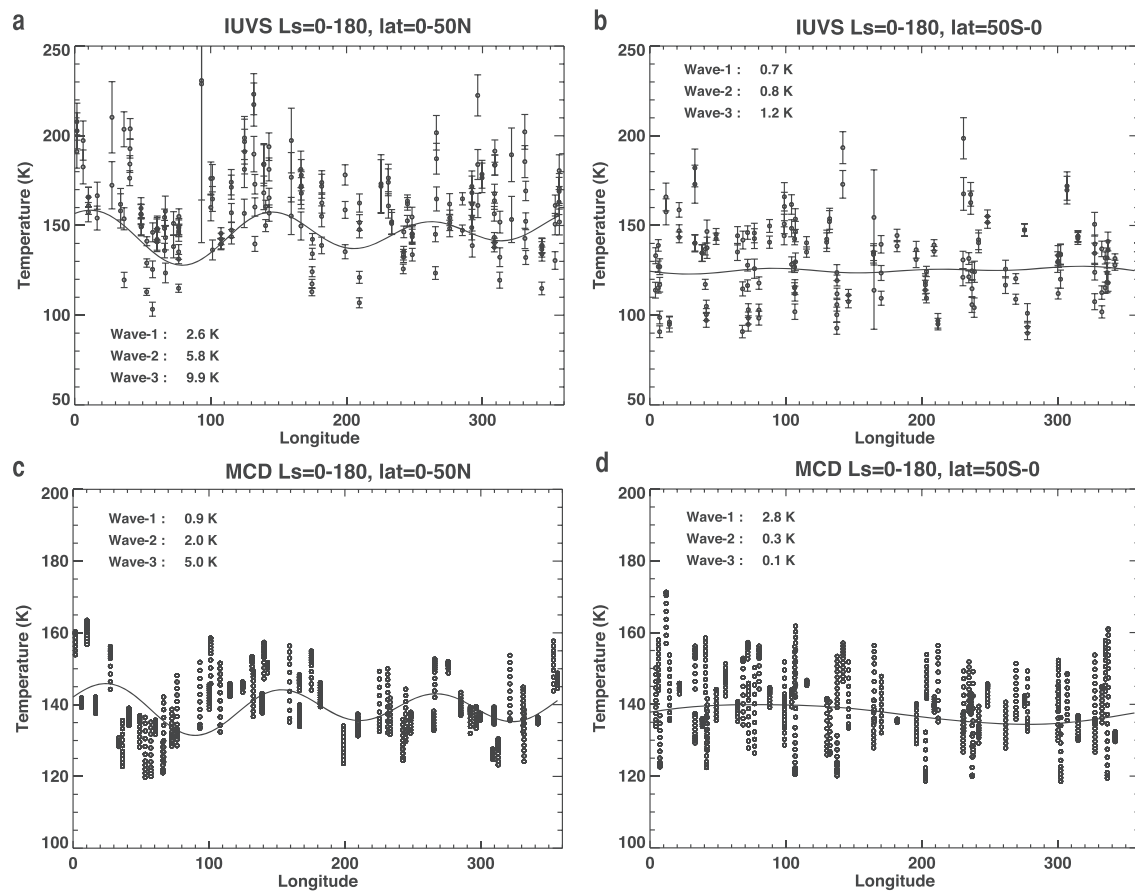


**Figure 4.** (a and b) Longitudinal variation of atmospheric temperature from Imaging Ultraviolet Spectrograph (IUVS) observations in altitudes between 75 and 85 km. The solid lines show the reconstruction of a total fit of wavenumber-0 to -3 to the data. The perturbation amplitudes for the wavenumber-1 to -3 components are shown in the figures. (c and d) The predictions by the Mars Climate Database are shown for corresponding geometries of IUVS. Uncertainties of IUVS temperature in northern and southern hemispheres are 7.1 and 5.6 K in average in the altitudes between 75 and 85 km. The standard deviation from the fit is (a) 28.7 K, (b) 22.2 K, (c) 10.3 K, and (d) 10.6 K, respectively.

mesosphere. The significant discrepancy of amplitudes between IUVS and MCD indicates that our current understanding of the Martian mesosphere remains incomplete. It is, however, noteworthy that the MCD predicts both the warm layer and wavenumber-3 structure but smaller than observed. These give us the mechanisms to understand, since the cause is presumably the same in the MCD and in the real Mars. In addition, the effect of internal gravity waves propagating from below may facilitate mesospheric heating via their momentum deposition (Medvedev & Yiğit, 2012). Another possible reason for the extra heating is the existence of an aerosol or haze layer in the mesospheric day side, as previously observed (Fedorova et al., 2014; Maltagliati et al., 2013; Montmessin et al., 2006). Such layers are potentially supplied from below, and from above as the meteoric layer (Crismani et al., 2017), that is not represented in models. This could effectively absorb incoming sunlight and contribute to localized heating on the dayside. This may potentially intensify the adiabatic heating in the subsidence of air on the nightside within the global circulation cell between the dayside and the nightside as a consequence of the mesospheric aerosol layer absorbing incoming sunlight. Our result suggests that the circulation pattern of Mars' mesosphere is reminiscent of the nightside warm layer detected on and interpreted by Bertaux et al. (2007) as the result of air subsidence of dayside-to-nightside circulation. As suggested by Stiepen et al. (2017) from NO nightglow observations, the circulation patterns of Mars from the summer dayside thermosphere to winter nightside thermosphere and mesosphere imply a strong dynamical coupling between mesosphere and thermosphere. Intensified transport may also explain the warm layer in the Martian mesosphere, while thermal tides and/or planetary waves modulate the amplitudes. It is noteworthy that a potential layer was also observed by SPICAM with a small amplitude around 80 km as seen in figure 16 in Forget

et al. (2009). The potential warm layer by SPICAM was observed at lower altitudes compared to this study. Further investigation of the global circulation in the mesosphere is crucial for identifying the heating source of the mesospheric warm layer.

The diurnal cycle could not be analyzed in detail because the data selected here were obtained on the nightside. Although stray light is a serious problem for dayside profiles, IUVS has nevertheless a capability to explore dayside (Gröller et al., 2018). Development of correction algorithms to reduce the stray light may eventually allow us to make improvements in our understanding of day-to-night variation in the Mars upper atmosphere. In addition, the atmospheric waves contributing the large variability can be better discriminated in LT coordinates. Examination of the  $L_s = 180\text{--}360^\circ$  period will be possible after analyzing data in the second half of Mars year.

This discovery may provide some insights into the mechanism helping to maintain water vapor in the mesosphere. Although the water vapor amount is not directly measured by IUVS, the interaction between water, aerosol, and background thermal structure could be solved in the near future by new observation by the Trace Gas Orbiter (Vandaele et al., 2019).

## 5. Conclusions

This paper presents a new set of stellar occultation measurements made using IUVS onboard MAVEN to reveal the nightside profiles of thermal structure in the middle atmosphere. We report the detection of a recurring layer of warm air between 70 and 90 km altitudes on the nightside in the northern hemisphere during  $L_s = 0\text{--}180^\circ$ . The predicted temperature at 80 km underestimates the observed temperature by up to 90 K. We have also discovered a wavenumber-3 structure with significant amplitudes that we interpret as signatures of thermal tides or planetary waves. MCD predicts the wavenumber-3 structure, although the contrast of warm layer amplitudes between the MCD and the IUVS is striking. A strong temperature inversion caused by a warm layer causes the convective instability layer in the mesosphere. This has potential impacts on the upward propagation of waves from below and consequently changes the background winds in the middle atmosphere. Our results highlight the dynamical nature of the mesospheric thermal structure and indicate the mesosphere poorly understood by current models.

## Acknowledgments

This work was supported by Grant-in-Aid for Scientific Research (A) 16H0229, 19H0707, Scientific Research (C) No. 19K03943, and No. 18H04453 from JSPS. The IUVS data are available from the PDS Archive. This work was conducted under NASA's MAVEN Participating Scientist Program (proposal #12-MAVENPS12-0017, PI: K. Seki). HN is supported by the Astrobiology Center Program of National Institutes of Natural Science (NINS) (Grant No. AB291015). HN would like to acknowledge Zachariah Milby for the assistance in evaluating this paper. All density and temperature profiles used in this study correspond to level 2, version 13, revision 1 data provided by the PDS ([https://pds-atmospheres.nmsu.edu/data\\_and\\_services/atmospheres\\_data/MAVEN/maven\\_iuvs.html](https://pds-atmospheres.nmsu.edu/data_and_services/atmospheres_data/MAVEN/maven_iuvs.html)).

## References

- Bertaux, J.-L., Koralev, O., Perrier, S., Quémérais, E., Montmessin, F., Leblanc, F., et al. (2006). SPICAM on Mars Express: Observing modes and overview of UV spectrometer data and scientific results. *Journal of Geophysical Research*, 111, E10S90. <https://doi.org/10.1029/2006JE002690>
- Bertaux, J.-L., Vandaele, A.-C., Koralev, O., Villard, E., Fedorova, A., Fussen, D., et al., & SPICAV/SOIR team (2007). A warm layer in Venus' cryosphere and high-altitude measurements of HF, HCl, H<sub>2</sub>O and HDO. *Nature*, 450. <https://doi.org/10.1038/nature05974>
- Bougher, S. W., Brain, J. L., Fox, F., Gonzalez-Galindo, C., & Simon-Wedlund, P. G. (2014). Withers, Upper neutral atmosphere and ionosphere. In *Mars Book II* (Chap. 14, pp. 433–463). Cambridge: Cambridge University Press.
- Bougher, P.-L., Blelly, M., Combi, M., Fox, J. L., Mueller-Wodarg, I., Ridley, A., & Roble, R. G. (2008). Neutral upper atmosphere and ionosphere modeling. *Space Science Reviews*, 139(1-4), 107–141. <https://doi.org/10.1007/s11214-008-9401-9>
- Bougher, S. W., Pawlowski, D., Bell, J. M., Nelli, S., McDunn, T., Murphy, J. R., et al. (2015). Mars global ionosphere-thermosphere model: Solar cycle, seasonal, and diurnal variations of the Mars upper atmosphere. *Journal of Geophysical Research, Planets*, 120, 311–342. <https://doi.org/10.1002/2014JE004715>
- Bougher, S. W., Roble, R. G., & Fuller-Rowell, T. (2002). Simulations of the upper atmospheres of the terrestrial planets. In M. Mendillo, A. Nagy & J. H. Waite (Eds.). *Atmospheres in the Solar System: Comparative Aeronomy*, *Geophys. Monogr. Ser* (Vol. 130, pp. 261–288). Washington, DC: AGU.
- Chaffin, M. S., Deighan, J., Schneider, N. M., & Stewart, A. I. F. (2017). elevated atmospheric escape of atomic hydrogen from Mars induced by high-altitude water. *Nature Geoscience*, 10(3), 174–178.
- Crismani, M. M., Schneider, N. M., Plane, J. M. C., Evans, J. S., Jain, S. K., Chaffin, M. S., et al. (2017). Detection of a persistent meteoric metallayer in the Martian atmosphere. *Nature Geoscience*, 10, 401. <https://doi.org/10.1038/ngeo2958>
- England, S. L., Liu, G., Kumar, A., Mahaffy, P. R., Elrod, M., Benna, M., et al. (2019). Atmospheric tides and high latitudes in the Martian upper atmosphere observed by MAVEN and MRO. *Journal of Geophysical Research, Space Physics*, 124, 2943–2953. <https://doi.org/10.1029/2019JA026601>
- England, S. L., Liu, G., Withers, P., Yiğit, E., Lo, D., Jain, S., et al. (2016). Simultaneous observations of atmospheric tides from combined in situ and remote observations at Mars from the MAVEN spacecraft. *Journal of Geophysical Research: Space Physics*, 121, 594–607. <https://doi.org/10.1002/2016JE004997>
- Fedorova, A. A., Bertaux, J.-L., Betsis, D., Montmessin, F., Koralev, O., Maltagliati, L., & Clarke, J. (2018). Water vapor in the middle atmosphere of Mars during the 2007 global dust storm. *Icarus*, 300, 440–457. <https://doi.org/10.1016/j.icarus.2017.09.025>
- Fedorova, A. A., Montmessin, F., Rodin, A. V., Koralev, O. I., Määttänen, A., Maltagliati, L., & Bertaux, J.-L. (2014). Evidence for a bimodal size distribution for the suspended aerosol particles on Mars. *Icarus*, 231, 239–260. <https://doi.org/10.1016/j.icarus.2013.12.015>
- Forbes, J. M., Bridger, A. F. C., Bougher, S. W., Hagan, M. E., Hollingsworth, J. L., Keating, G. M., & Murphy, J. (2002). Non-migrating tides in the thermosphere of Mars. *Journal of Geophysical Research*, 107(E11), 5113. <https://doi.org/10.1029/2001JE001582>

- Forget, F., Hourdin, F., Fournier, R., Hourdin, C., Talagrand, O., Collins, M., et al. (1999). Improved general circulation models of the Martian atmosphere from the surface to above 80 km. *Journal of Geophysical Research*, 104, 24,155–24,176.
- Forget, F., Montmessin, F., Bertaux, J.-L., González-Galindo, F., Lebonnois, S., Quémérais, E., et al. (2009). Density and temperature of the upper Martian atmosphere measured by stellar occultations with Mars Express SPICAM. *Journal of Geophysical Research*, 114, E01004. <https://doi.org/10.1029/2008JE003086>
- Fritts, D. C., & Alexander, M. J. (2003). Gravity wave dynamics and effects in the middle atmosphere. *Reviews of Geophysics*, 41(1), 1003. <https://doi.org/10.1029/2001RG000106>
- Gonzalez-Galindo, F., Chaufray, J.-Y., Forget, F., García-Comas, M., Montmessin, F., Jain, S. K., & Stiepen, A. (2018). UV dayglow variability on Mars: Simulation with a global climate model and comparison with SPICAM/MEX Data. *Journal of Geophysical Research, Planets*, 123, 1934–1952. <https://doi.org/10.1029/2018JE005556>
- Gonzalez-Galindo, F., Lopez-Valverde, M. A., Forget, F., García-Comas, M., Millour, E., & Montabone, L. (2015). Variability of the Martian thermosphere during eight Martian years as simulated by a ground-to-exosphere global circulation model. *Journal of Geophysical Research, Planets*, 120, 2020–2035. <https://doi.org/10.1002/2015JE004925>
- Grassi, D., Fiorenza, C., Zasova, L. V., Ignatiev, N. I., Maturilli, A., Formisano, V., & Giuranna, M. (2005). The Martian atmosphere above great volcanoes: Early planetary Fourier spectrometer observations. *Planetary and Space Science*, 53, 1053–1064.
- Gröller, H., Montmessin, F., Yelle, R. V., Lefèvre, F., Forget, F., Schneider, N. M., et al. (2018). MAVEN/IUVS stellar occultation measurements of Mars atmospheric structure and composition. *Journal of Geophysical Research, Planets*, 123, 1449–1483. <https://doi.org/10.1029/2017JE005466>
- Gröller, H., Yelle, R. V., Koskinen, T. T., Montmessin, F., Lacombe, G., Schneider, N. M., et al. (2015). Probing the Martian atmosphere with MAVEN/IUVS stellar occultations. *Geophysical Research Letters*, 42, 9064–9070. <https://doi.org/10.1002/2015GL065294>
- Heavens, N. G., Kleinböhl, A., Chaffin, M. S., Halekas, J. S., Kass, D. M., Hayne, P. O., et al. (2018). Hydrogen escape from Mars enhanced by deep convection in dust storms. *Nature Astronomy*, 2(2), 126–132. <https://doi.org/10.1038/s41550-017-0353-4>
- Heavens, N. G., Richardson, M. I., Lawson, W. G., Lee, C., McCleese, D. J., Kass, D. M., et al. (2010). Convective instability in the martian middle atmosphere. *Icarus*, 208, 574–589. <https://doi.org/10.1016/j.icarus.2010.03.023>
- Hinson, D. P., Smith, M. D., & Conrath, B. J. (2004). Comparison of atmospheric temperatures obtained through infrared sounding and radio occultation by Mars Global Surveyor. *Journal of Geophysical Research*, 109, E12002. <https://doi.org/10.1029/2004JE002344>
- Keating, G. M., Bouger, S. W., Theriot, M. E., Tolson, R. H., Zurek, R. W., Blanchard, R. C., et al. (2007). Mars neutral Upper atmosphere temporal and spatial variations discovered from the accelerometer science experiment aboard Mars Reconnaissance Orbiter, *Lunar Planet. Sci.*, XXXVIII, 2074.
- Keating, G. M., Bouger, S. W., Zurek, R. W., Tolson, R. H., Cancro, G. J., Noll, S. N., et al. (1998). The structure of the upper atmosphere of mars: In situ accelerometer measurements from Mars Global Surveyor. *Science*, 279(5357), 1672–1676. <https://doi.org/10.1126/science.279.5357.1672>
- Keating, G. M., Theriot, M. Jr., Tolson, R., Bouger, S., Forget, F., & Forbes, J. (2003). Global measurements of the Mars upper atmosphere: In situ accelerometer measurements from Mars Odyssey 2001 and Mars Global Surveyor, *Lunar Planet. Sci.*, XXXIV, 1142.
- Lebonnois, S., Quémérais, E., Montmessin, F., Lefèvre, F., Perrier, S., Bertaux, J.-L., & Forget, F. (2006). Vertical distribution of ozone on Mars as measured by SPICAM/Mars Express using stellar occultations. *Journal of Geophysical Research*, 111, E09S05. <https://doi.org/10.1029/2005JE002643>
- Määttänen, A., Lefèvre, F., Montmessin, F., Listowski, C., Guilbon, S., Fedorova, A., & Koralev, O. (2019). Climatology of the ozone vertical distribution on Mars from SPICAM/MEX UV occultations. *Icarus*. <https://doi.org/10.1016/j.icarus.2019.113428>
- Määttänen, A., Listowski, C., Montmessin, F., Maltagliati, L., Reberac, A., Joly, L., & Bertaux, J.-L. (2013). A complete climatology of the aerosol vertical distribution on Mars from MEX/SPICAM UV solar occultations. *Icarus*, 223, 892–941. <https://doi.org/10.1016/j.icarus.2012.12.001>
- Magalhães, J. A., Schofield, J. T., & Seiff, A. (1999). Results of the Mars Pathfinder atmospheric structure investigation. *Journal of Geophysical Research*, 104, 8943–8955.
- Maltagliati, L., Montmessin, F., Fedorova, A., Koralev, O., Forget, F., & Bertaux, J. L. (2011). Evidence of water vapor in excess of saturation in the atmosphere of Mars. *Science*, 333, 1868. <https://doi.org/10.1126/science.1207957>
- Maltagliati, L., Montmessin, F., Koralev, O., Fedorova, A., Forget, F., Määttänen, A., et al. (2013). Annual survey of water vapor vertical distribution and water-aerosol coupling in the Martian atmosphere observed by SPICAM/MEX solar occultations. *Icarus*, 223, 942–962.
- McCleese, D. J., Schofield, J. T., Taylor, F. W., Calcutt, S. B., Foote, M. C., Kass, D. M., et al. (2007). Mars Climate Sounder: An investigation of thermal and water vapor structure, dust and condensate distributions in the atmosphere, and energy balance of the polar regions. *Journal of Geophysical Research*, 112(E5), E05S06. <https://doi.org/10.1029/2006JE002790>
- McCleese, D. J., Schofield, J. T., Taylor, F. W., Abdou, W. A., Aharonson, O., Banfield, D., et al. (2008). Intense polar temperature inversion in the middle atmosphere on Mars. *Nature Geoscience*, 1(11), 745–749. <https://doi.org/10.1038/ngeo332>
- McClintock, W. E., Schneider, N. M., Holsclaw, G. M., Clarke, J. T., Hoskins, A. C., Stewart, I., et al. (2014). The Imaging Ultraviolet Spectrograph (IUVS) for the MAVEN mission. *Space Science Reviews*, 195(1–4), 75–124. <https://doi.org/10.1007/s11214-014-0098-7>
- Medvedev, A. S., & Yiğit, E. (2012). Thermal effects of internal gravity waves in the Martian upper atmosphere. *Geophysical Research Letters*, 39, L05201. <https://doi.org/10.1029/2012GL050852>
- Millour, E., Spiga, A., Colaitis, A., Navarro, T., Madeleine, J.-B., Chaufray, J.-Y., et al. (2012). Mars Climate Database Version 5, in: European Planetary Science Congress 2012. p. 302.
- Modak, A., Sheel, V., & Montmessin, F. (2019). Retrieval of Martian ozone and dust from SPICAM spectrometer for MY27–MY28. *Journal of Earth System Science*, 128(6), 1–14. <https://doi.org/10.1007/s12040-019-1167-9>
- Montmessin, F., Koralev, O., Lefèvre, F., Bertaux, J. L., Fedorova, A., Trokhimovskiy, A., et al. (2017). SPICAM on Mars Express: A 10 year in-depth survey of the Martian atmosphere. *Icarus*, 297, 195–216.
- Montmessin, F., Quémérais, E., Bertaux, J. L., Koralev, O., Rannou, P., & Lebonnois, S. (2006). Stellar occultations at UV wavelengths by the SPICAM instrument: Retrieval and analysis of Martian haze profiles. *Journal of Geophysical Research*, 111, E09S09. <https://doi.org/10.1029/2005JE002662>
- Pätzold, M., Häusler, B., Tyler, G. L., Andert, T., Asmar, S. W., Bird, M. K., et al. (2016). Mars Express 10 years at Mars: Observations by the Mars Express Radio Science Experiment (MaRS). *Planetary and Space Science*, 127, 44–90. <https://doi.org/10.1016/j.pss.2016.02.013>
- Quémérais, E., Bertaux, J.-L., Koralev, O., Dimarellis, E., Cot, C., Sandel, B. R., & Fussen, D. (2006). Stellar occultations observed by SPICAM on Mars Express. *Journal of Geophysical Research*, 111, E09S04. <https://doi.org/10.1029/2005JE002604>
- Sandel, B. R., Gröller, H., Yelle, R. V., Koskinen, T., Lewis, N. K., Bertaux, J.-L., et al. (2015). Altitude profiles of O<sub>2</sub> on Mars from SPICAM stellar occultations. *Icarus*, 252, 154–160. <https://doi.org/10.1016/j.icarus.2015.01.004>

- Seiff, A., & Kirk, D. B. (1977). Structure of the atmosphere of mars in summer at mid-latitudes. *Journal of Geophysical Research*, 82(28), 4364–4378.
- Smith, M. D. (2004). Interannual variability in TES atmospheric observations of Mars during 1999–2003. *Icarus*, 167, 148–165.
- Smith, M. D., Pearl, J. C., Conrath, B. J., & Christensen, P. R. (2001). Thermal Emission Spectrometer results: Mars atmospheric thermal structure and aerosol distribution. *Journal of Geophysical Research*, 106, 23,929–23,945.
- Stiepen, A., Jain, S. K., Schneider, N. M., Deighan, J. I., González-Galindo, F., Gérard, J.-C., et al. (2017). Nitric oxide nightglow and Martian mesospheric circulation from MAVEN/IUVS observations and LMD-MGCM predictions. *Journal of Geophysical Research: Space Physics*, 122, 5782–5797. <https://doi.org/10.1002/2016JA023523>
- Vandaele, A. C., Koralev, O., Daerden, F., Aoki, S., Thomas, I. R., Altieri, F., et al., NOMAD Science Team, & ACS Science Team (2019). Martian dust storm impact on atmospheric H<sub>2</sub>O and D/H observed by ExoMars Trace Gas Orbiter. *Nature*, 568(7753), 521–525. <https://doi.org/10.1038/s41586-019-1097-3>
- Withers, P., & Smith, M. D. (2006). Atmospheric entry profiles from the Mars Exploration Rovers Spirit and Opportunity. *Icarus*, 185, 133–142.
- Withers, P., Bertaux, J.-L., & Montmessin, F. (2011). Observations of thermal tides in the middle atmosphere of Mars by the SPICAM instrument. *Journal of Geophysical Research*, 116, E1105. <https://doi.org/10.1029/2011JE003847>